UNIVERSITÀ DEGLI STUDI FIRENZE

FLORE
Repository istituzionale dell'Università degli Studi di Firenze

Formation and properties of amorphous magnesium-calcium phosphate particles in a simulated intestinal fluid

Questa è la Versione finale referata (Post print/Accepted manuscript) della seguente pubblicazione:

Original Citation:

Formation and properties of amorphous magnesium-calcium phosphate particles in a simulated intestinal fluid / Gelli, Rita; Tempesti, Paolo; Ridi, Francesca*; Baglioni, Piero. - In: JOURNAL OF COLLOID AND INTERFACE SCIENCE. - ISSN 0021-9797. - ELETTRONICO. - 546(2019), pp. 130-138. [10.1016/j.jcis.2019.03.060]

Availability:

This version is available at: 2158/1152116 since: 2019-04-02T15:34:09Z

Published version:

DOI: 10.1016/j.jcis.2019.03.060

Terms of use:

Open Access

La pubblicazione è resa disponibile sotto le norme e i termini della licenza di deposito, secondo quanto stabilito dalla Policy per l'accesso aperto dell'Università degli Studi di Firenze (https://www.sba.unifi.it/upload/policy-oa-2016-1.pdf)

Publisher copyright claim:

(Article begins on next page)

10 January 2022

Accepted Manuscript

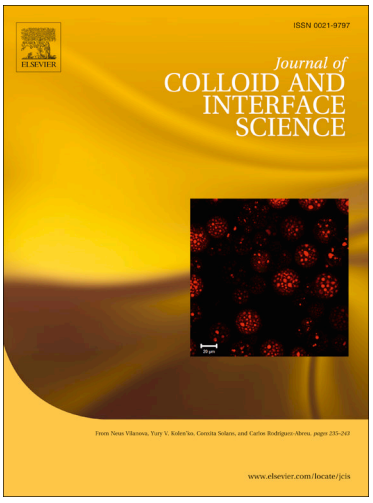

Formation and properties of amorphous magnesium-calcium phosphate particles in a simulated intestinal fluid

Rita Gelli, Paolo Tempesti, Francesca Ridi, Piero Baglioni

PII: S0021-9797(19)30358-3
DOI: https://doi.org/10.1016/j.jcis.2019.03.060
Reference: YJCIS 24781

To appear in: *Journal of Colloid and Interface Science*

Received Date: 15 January 2019
Revised Date: 12 March 2019
Accepted Date: 18 March 2019

Please cite this article as: R. Gelli, P. Tempesti, F. Ridi, P. Baglioni, Formation and properties of amorphous magnesium-calcium phosphate particles in a simulated intestinal fluid, *Journal of Colloid and Interface Science* (2019), doi: https://doi.org/10.1016/j.jcis.2019.03.060

This is a PDF file of an unedited manuscript that has been accepted for publication. As a service to our customers we are providing this early version of the manuscript. The manuscript will undergo copyediting, typesetting, and review of the resulting proof before it is published in its final form. Please note that during the production process errors may be discovered which could affect the content, and all legal disclaimers that apply to the journal pertain.

ACCEPTED MANUSCRIPT

Formation and properties of amorphous magnesium-calcium phosphate particles in a simulated intestinal fluid

Rita Gelli, Paolo Tempesti, Francesca Ridi*, Piero Baglioni

Department of Chemistry "Ugo Schiff" and CSGI, University of Florence, via della Lastruccia 3, 50019 Sesto Fiorentino, Florence, Italy

Corresponding author at: Department of Chemistry "Ugo Schiff" and CSGI, University of Florence, via della Lastruccia 3, Sesto Fiorentino, 50019 Florence, Italy.
E-mail: francesca.ridi@unifi.it

Abstract

Hypothesis: the endogenous self-assembly of amorphous magnesium-calcium phosphate (AMCP) nanoparticles in human small intestine is an intriguing and newly-discovered process involved in immune-surveillance mechanisms. The study of nano and microparticles formation in complex media mimicking *in vivo* conditions contributes to unravel the features of endogenous AMCPs and, from a physico-chemical perspective, to shed light on the effect of biorelevant molecules on the precipitation of AMCPs.

Experiments: endogenous-like AMCPs have been synthesized in a commercial simulated intestinal fluid (SIF), which contains biorelevant molecules such as lecithin and taurocholate. The properties of these particles were compared to the features of AMCPs synthesized in water. The stability of the amorphous phase as a function of time, as well as AMCPs' morphology, have been investigated. In particular, the effect of the organic molecules present in the SIF was examined in terms of incorporation in the nano and micro particles and on their nanoscale structure.

Findings: taurocholate and lecithin, present in the SIF, enhance stability of amorphous phase against particles crystallization, and lead to the formation of smaller AMCP aggregates with a rougher surface. They are also incorporated in the inorganic phase, and their self-assembled structure leads to the formation of core-shell nanoparticles.

Abbreviations: CaPs: Calcium Phosphates; AMCP: Amorphous Magnesium-Calcium Phosphate; AMP: Amorphous Magnesium Phosphate; ACP: Amorphous Calcium Phosphate; GI: Gastrointestinal; SIF: Simulated Intestinal Fluid; HA: Hydroxyapatite; PC: Phosphatidylcholine; DLS: Dynamic Light Scattering; CMC: Critical Micelle Concentration FT-IR: Fourier Transform-Infrared Spectroscopy; XRD: X-Rays Diffraction; PDF: Powder Diffraction File; FE-SEM: Field Emission-Scanning Electron Microscopy; TEM: Transmission Electron Microscopy; SAXS: Small Angle X-Rays Scattering.

ACCEPTED MANUSCRIPT

Graphical Abstract

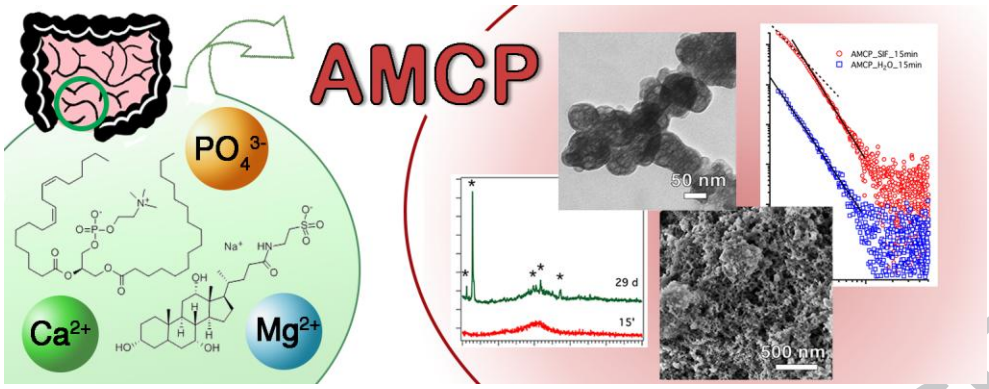

Keywords (max. 10)
Amorphous Magnesium-Calcium Phosphate; Gut; Simulated Intestinal Fluids; Lecithin; Taurocholate; Self-assembly; Stability; Porosity; Nanostructure.

1. Introduction

The *in vivo* formation of biogenic calcium phosphates (CaPs) is regulated by relevant biomolecules controlling the self-assembly process typical of Soft Matter [1]. The most notable example is the process of bone biomineralization, in which the deposition of platelet-like apatitic nanocrystals is templated by the collagen I fibers' network formed through self-assembly [2]. Other examples include the role of amelogenin on the regulation of carbonated apatite crystalline 3D network in enamel [3] and the action of the protein fetuin-A in complexing amorphous calcium phosphate clusters in serum [4]. Another scenario where the formation of CaP-based minerals occurs in a complex biological environment is the small intestine. It has been recently shown that in the ileum region of the human gut, the endogenous secretions of calcium and phosphate ions from the distal small intestine into the lumen lead to the precipitation of amorphous magnesium-substituted calcium phosphate particles (AMCPs) [5]. These particles trap macromolecules, *i.e.* orally fed protein antigens and bacterial peptidoglycans, and transport them to the immune cells of the intestinal tissue, promoting the immuno-surveillance mechanisms. Endogenous AMCPs are porous and composed by agglomerates of small nanoparticulate structures; the amorphous nature allows for the effective incorporation of the organic cargo, as it was shown during *in vitro* experiments [6].

The study of amorphous magnesium and calcium phosphates is particularly relevant. On the one hand, amorphous magnesium phosphates (AMPs) constitute an emerging field of research: together with crystalline magnesium phosphates, these components represent relatively new biocompatible

ACCEPTED MANUSCRIPT

options for the preparation of nanostructured biomaterials [7–10]. On the other hand, amorphous calcium phosphates (ACPs) have been extensively investigated in the past for their interesting properties [11,12]; moreover, it is known that, both *in vivo* and *in vitro*, their structure and stability are sensitive to many physico-chemical properties (temperature, pH, viscosity, ionic strength, presence of foreign ions and molecules [11–14]) of the medium in which they form. The determination of these properties in human ileum is challenging, since intestinal fluids are prone to a large variability in their composition [15]. Moreover, the majority of literature studies are devoted to the duodenal and jejunal composition, and the features of the lower part of the gastrointestinal tract (GI), such as the ileum where AMCPs form, are often neglected [16,17].

The development of standardized simulated fluids that mimic the different regions of the GI tract is of outmost importance, especially in the assessment of the dissolution and solubility of drugs. Nowadays, some biorelevant simulated intestinal fluids (SIF) are commercially available. These media typically consist of aqueous solutions of bile salts (anionic natural steroidal surfactants, typically sodium taurocholate) and phospholipids (such as lecithin, a mixture of phosphatidylcholines), in addition to other components that allow the fluid to mimic the pH, the osmolality and the buffer capacity of each specific tract of the gut [18,19]. The simultaneous presence in solution of bile salts and lecithin often results in the formation of self-assembled structures, such as mixed micelles, depending on their molar ratio, concentration, pH, ionic strength and temperature [19,20]. In the mixed micelles, which are also present *in vivo* and allow for the solubilization and absorption of dietary fats [21], bile salts are located between polar head groups of phospholipids, with their hydrophilic sides exposed to the aqueous environment; this results in the formation of either spherical, cylindrical or worm-like micelles, with sizes ranging from 3.5 to 70 nm, depending on the phospholipid and bile salt amount and their ratio [19,21–25]. To the best of our knowledge, the detailed characterization of the fluid which mimics specifically the ileum region of the intestine [18] has never been reported.

Given the presence of endogenous AMCP nanoparticles in the distal small intestine, understanding the formation mechanism of CaPs in a complex fluid that simulates the *in vivo* conditions is particularly relevant. Even though AMCP formation in SIF has never been investigated so far, the literature reports some examples about the effect of the separate components, *i.e.* taurocholate and lecithin, on the formation of CaP-based materials. Bile can inhibit the formation of CaP, likely because of the action of bile salt/phospholipid micelles [26]. It was suggested that Ca^{2+} interaction with both free and micellar taurocholate anions is responsible for the inhibitory effect, as it limits Ca^{2+} concentration and potentially acts as buffer against the precipitation of calcium-containing gallstones [27]. Moreover, different bile salts have a different inhibitory effect [28]. The effect of

ACCEPTED MANUSCRIPT

mixed taurodeoxycholate/phosphatidylcholine (PC) micelles on hydroxyapatite (HA) binding and precipitation inhibition was also investigated, showing that the ability to delay HA formation/ precipitation is dependent on the composition of the micelles [26,29].

The effect of lecithin on calcium phosphate formation was explored to a lesser extent. Recently, soybean lecithin was used as a template to prepare ACP porous hollow microspheres [30], while Michał *et al.* obtained HA nanoparticles using of a lecithin-based wet chemical precipitation method [31].

In a previous work, we investigated the effect of pH and Mg^{2+} concentration on the amorphous phase stability of endogenous-like AMCPs [14]. We thoughtfully characterized the physico-chemical properties of the obtained particles, and we related the variation of the cited parameters (which are known to have implications in gut health) to the lifetime of the amorphous phase in solution. In the attempt of gaining new insights in the *in vivo* formation process and stability, the present work reports on the formation and the features of endogenous-like AMCPs prepared in a simulated intestinal fluid. We believe that these results have a two-fold relevance, as they shed light on the effect of sodium taurocholate and lecithin on the precipitation of amorphous calcium and magnesium phosphates, relevant for the *in vivo* formation and features of AMCPs.

2. Materials and methods

2.1 Materials

The powder "FaSSIF/FeSSIF/FaSSGF" used to prepare the Simulated Intestinal Fluid (SIF) was purchased from Biorelevant.com Ltd (London, UK). Sodium chloride (NaCl, ≥ 99%), maleic acid ($C_4H_4O_4$, ≥ 99%), magnesium chloride ($MgCl_2 \cdot 6H_2O$, ≥ 99%) calcium chloride ($CaCl_2$, ≥ 93%) and NaOH pellets were purchased from Sigma-Aldrich (Milan, Italy). Sodium phosphate monobasic ($NaH_2PO_4 \cdot H_2O$, ≥ 99%), and sodium phosphate dibasic ($Na_2HPO_4 \cdot 12H_2O$, ≥ 99%) were obtained from Carlo Erba Reagents (Milan, Italy). Deionized water was used during all the experiments.

2.2 Preparation of the Simulated Intestinal Fluid

The SIF specifically mimicking the ileum region of the gut was prepared according to the instructions given by the supplier. 500 mL of the fluid were prepared by dissolving 0.880 g of NaCl, 3.065 g of maleic acid and 2.115 g of NaOH in deionized water (450 mL). A solution of NaOH 2 M was used to adjust the pH at 7.5, then we made up to the final volume with water. 0.3 g of powder (FaSSIF/FeSSIF/FaSSGF) were dissolved in the prepared buffer, and the fluid was let stand for at least 2 h before use. The medium was used within 24 h from the preparation. The final

ACCEPTED MANUSCRIPT

concentrations of the components are: sodium taurocholate 0.8 mM, lecithin 0.2 mM and maleic acid 52.8 mM [18].

2.3 Synthesis of AMCP in water and in SIF

AMCP was obtained by mixing equal volumes (200 mL) of two solutions, namely solution A (which contains NaCl, $MgCl_2$ and $CaCl_2$, amounts and concentrations listed in Table S1 in the Supplementary Material) and solution B (NaH_2PO_4 and Na_2HPO_4, see Table S1) [32]. The ionic concentrations used are consistent with the ones typical of ileum [33]. Two syntheses were conducted using the same procedure, except for the fact that the salts were dissolved in SIF or water. Solution A and B were separately heated at 37 °C in a water bath. Solution A was added to solution B and the pH was adjusted to 7.50, which is representative of the ileum region [34], by dropwise addition of NaOH 2 M. Aliquots of the solution (~20 mL) were periodically withdrawn from the reaction flask and filtered using a Millipore vacuum filtration system equipped with mixed cellulose esters filters (Millipore, pore size 0.22 μm). Filters were immediately placed in plastic test tubes and frozen in liquid nitrogen, prior to lyophilization for 24 h. As a preventive measure, particles were stored at -18 °C, tightly closed to prevent any influence from environmental humidity which could lead to spontaneous crystallization.

2.4 Characterization techniques

2.4.1 Dynamic Light Scattering (DLS)

DLS measurements were performed on a Brookhaven Instruments apparatus (BI 9000AT correlator and BI 200 SM goniometer). The light source was a Torus laser, mpc3000, LaserQuantum, UK (λ = 532 nm) and the scattered intensity was detected by a BI-APD detector. The samples were placed in glass tubes and immersed in a thermostated cell at 37 °C filled with decahydronaphthalene to match the glass refractive index. The scattering intensity of pure toluene was used as a standard. The field autocorrelation functions reported in this work are the result of the averaging of five experiments for each sample. The averaged functions were analyzed through cumulant analysis (see Supplementary Material for details).

2.4.2 Surface Tension

The surface tension properties of the SIF were determined using a Force Tensiometer K100 (Krüss GmbH, Hamburg, Germany). Inverse critical micelle concentration (CMC) measurements were performed using a Pt plate, at T = 37 °C and diluting the sample with water up to $1 \cdot 10^{-5}$ mM sodium taurocholate concentration.

2.4.3 Fourier Transform Infrared Spectroscopy (FT-IR)

ACCEPTED MANUSCRIPT

FT-IR spectra were collected using a Bio-Rad FTS-40 spectrophotometer (Hercules, CA, USA). The samples were analyzed in KBr pellets, prepared by mixing 1.00 ± 0.05 mg of sample with 100 ± 1 mg of KBr (Sigma-Aldrich, FT-IR grade). The spectra were acquired in the range 4000-400 cm^{-1} using a resolution of 2 cm^{-1}, 64 scans and scan delay of 600 s.

2.4.4 X-Rays Diffraction (XRD)

X-rays Diffraction (XRD) patterns were collected with a D8 Advance with DAVINCI design (Bruker, Milan, Italy), using as X-rays source the Cu Kα radiation (wavelength λ=1.54 Å), at 40 kV and 40 mA, a 2θ range of 5°-60°, a step size of 0.03°, and a time/step of 0.3 s. A Si zero-background sample holder was used, while peaks' assignment was based on the Powder Diffraction Files (PDF) of the ICDD database (International Centre for Diffraction Data).

2.4.5 Field Emission-Scanning Electron Microscopy (FE-SEM)

Field Emission-Scanning Electron Microscopy (FE-SEM) analysis was conducted using a Zeiss ΣIGMA FE-SEM (Carl Zeiss Microscopy GmbH, Jena, Germany). The powders were placed over aluminum stubs by means of conductive tape. The micrographs were acquired with an accelerating voltage of 2 kV, sample-detector distance ~ 2 mm and using the In-Lens detector.

2.4.6 Simultaneous Thermogravimetry/ Differential Scanning Calorimetry

Simultaneous Thermogravimetry/ Differential Scanning Calorimetry analyses were performed using SDT Q600 from TA Instruments (New Castle, DE, USA). Each sample was placed in an alumina pan and measurements were conducted in N_2 atmosphere (flow rate 100 mL/min) from room temperature to 1000 °C, at 10 °C/min.

2.4.7 Transmission Electron Microscopy (TEM)

Transmission Electron Microscopy (TEM) analysis of AMCPs was performed with a TEM Philips CM12 (Eindhoven, The Netherlands), working with an electron gun operating at 100 kV. Samples were prepared by depositing a droplet of a sonicated AMCPs dispersion in ethanol onto a carbon-coated copper grid.

2.4.8 Small Angle X-Rays Scattering (SAXS)

SAXS measurements were carried out using a HECUS SWAX- camera (Kratky) equipped with a position-sensitive detector (OED 50 M) containing 1024 channels of width 54 µm. Cu K_α radiation of wavelength λ = 1.542 Å was provided using a Seifert ID-3003 X-ray generator (sealed-tube type), operating at a maximum power of 2 kW. A 10-mm thick Ni-filter was used to remove Cu K_β radiation. The sample-to-detector distance was 275 mm. The volume between the sample and the detector was kept under vacuum during the measurements to minimize scattering from the air. The Kratky camera was calibrated in the small angle region using silver behenate (d = 5.838 nm). Scattering curves were obtained in the Q-range, $Q = (4\pi/\lambda)\sin(\theta/2)$, between 0.009 and 0.54 $Å^{-1}$,

ACCEPTED MANUSCRIPT

with Q being the scattering vector, and θ the scattering angle. The samples were contained in 2 mm quartz capillaries. Standard measurement conditions were 40 kV, 20 mA, and 3 h (acquisition time) at 25 °C. SAXS curves reported in this work have been compared with those obtained on very short time scales and no differences were detectable between the two sets of measurements. All scattering curves were corrected for the solvent/empty cell contribution considering the relative transmission factor. SAXS curves were iteratively desmeared using the procedure reported by Lake [35]. The interpretation of the curves was carried out with a power law model associated to the linear regions in the double log representation (Eq. 1):

$$I(q) = A\, q^{-p} \quad (1)$$

where A is a scale factor and p is the slope of the linear fitting. When $1 \leq p \leq 3$, p represents the mass-fractal dimension (D_m) that is 3 for full solid materials [36]. When $3 \leq p \leq 4$ one can calculate the surface-fractal dimension (D_s) from the equation:

$$D_s = 6 - p \quad (2)$$

Typically, D_s is 2 for smooth surfaces, and goes towards 3 as the roughness increases [37].

3. Results and discussion

3.1 SIF characterization

DLS was employed to investigate the presence of self-assembled aggregates in the SIF. Cumulant analysis of the autocorrelation function (Figure S1 in the Supplementary Material) revealed the presence of nanosized objects with a mean hydrodynamic radius of 17 nm and high polydispersity (0.28), in good accordance with previously synthesized taurocholate-lecithin colloids [19].

As DLS revealed the presence of nanosized objects in the fluid, the interfacial properties of the medium were examined by means of force tensiometry. We found that the SIF does not show a CMC, as the surface tension does not display a steep decrease at a given concentration value (data not shown). Again, this is in agreement with the literature, as many data suggest that for bile salts the transition from monomeric to micellar solution occurs stepwise over a broad range of concentrations [20,27].

3.2 AMCP stability

ACCEPTED MANUSCRIPT

We assessed the stability of AMCPs prepared in the SIF and in water, to evaluate the effect of the taurocholate and lecithin on the nano/microparticles crystallization process. Given that amorphous calcium and magnesium phosphates are well-known to spontaneously crystallize in aqueous solution [11,38], the conversion kinetics of amorphous calcium phosphate to crystalline material was monitored through the analysis of the particles by means of FT-IR spectroscopy and XRD patterns, see Figure 1.

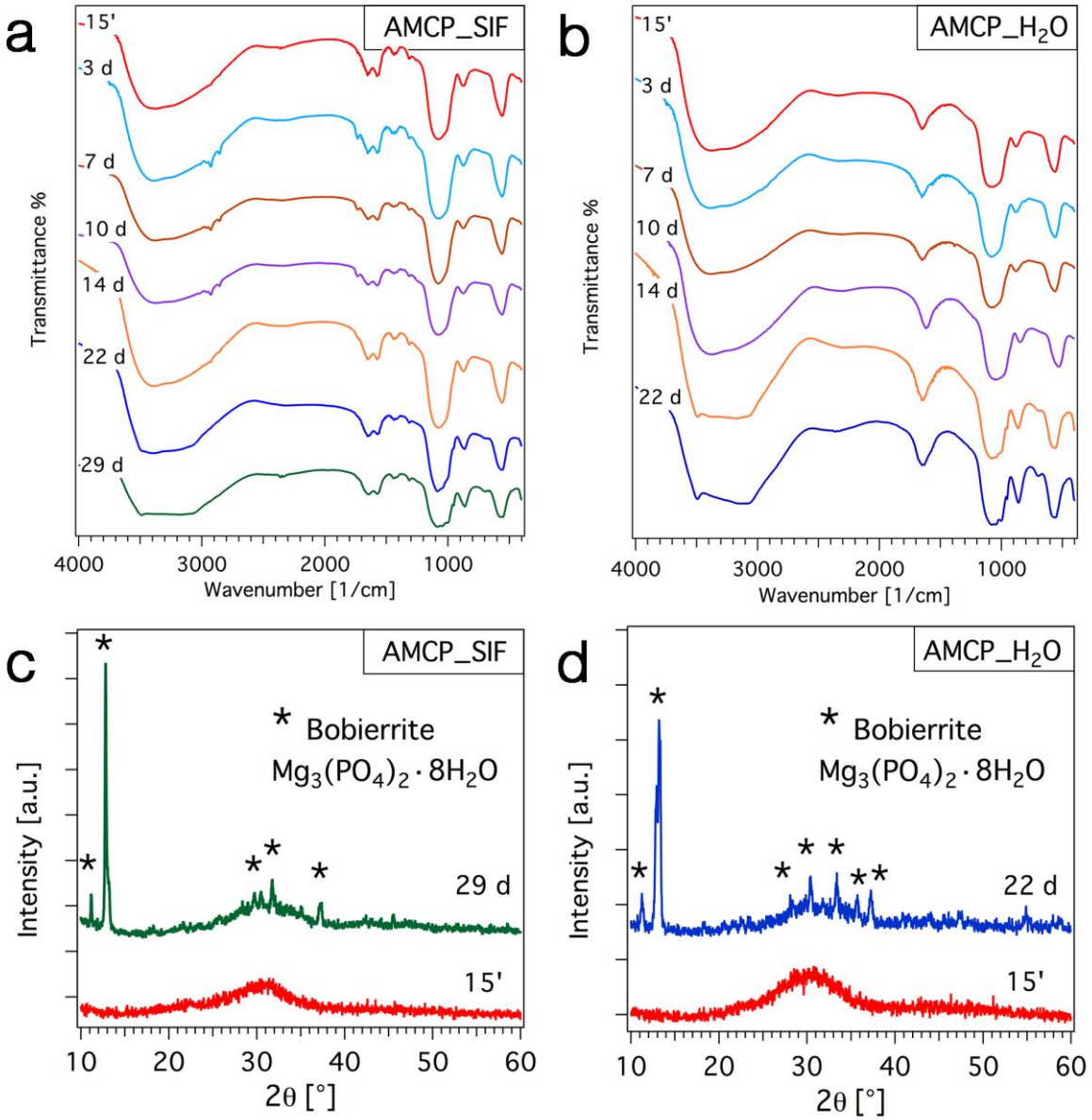

Fig. 1: (a,b) FT-IR spectra of AMCPs synthesized in (a) SIF and (b) water; the spectra are offset for display purposes; c) XRD patterns of AMCPs_SIF collected after 15 min and 29 days of reaction; d) XRD patterns of AMCPs_H_2O collected after 15 min and 22 days of reaction. The diffractograms are offset for display purposes. The PDF of Bobierrite is [33-0878].

The shape and the position of the IR peaks reveal that, in both SIF and water syntheses, the initially formed precipitate is an amorphous phosphate [11,38–41] (for a more detailed peaks' assignment of

ACCEPTED MANUSCRIPT

AMCP, the reader is referred elsewhere [14]). The kinetic stability of the amorphous phase is different depending on the reaction medium: when AMCPs are prepared in the SIF (Fig. 1a), the ν_3 phosphate stretching peak (~1080 cm^{-1}) appears slightly split after 22 days, while AMCPs synthesized in water turn crystalline after 14 days (see Fig. 1b, orange spectrum). The shape of the O-H stretching band (2700-3700 cm^{-1}) also evolves in time, and a sharp peak at 3488 cm^{-1} appears. The nature of the crystalline phase formed upon conversion of AMCPs was investigated by means of XRD analysis (see Fig. 1c and d). The XRD patterns of the 29-day product in SIF and the 22 day-product in water are displayed in Figure 1c and 1d, respectively, as they represent the most aged samples collected during the syntheses. For both synthetic pathways, we can observe that the product collected after 15 min is amorphous (broad hump centered at ~32° [41]) and converts to crystalline bobierrite ($Mg_3(PO_4)_2 \cdot 8H_2O$, PDF 33-0878). The lack of formation of crystalline CaP phases is likely due to the presence of Mg^{2+} in solution, which strongly hinders ACP crystallization [13,14,42]; moreover, the conversion of amorphous phosphates containing Mg to bobierrite was already reported in the literature [10,43]. The FT-IR spectra of the crystalline samples (green curve in Fig. 1a and blue curve in Fig. 1b) are also consistent with the presence of bobierrite [44]. From the difference in the crystallization temporal intervals in the two synthetic media, we can conclude that the lifetime of the amorphous phase of AMCPs in enhanced when they are prepared in the SIF, suggesting a stabilizing action of sodium taurocholate and/or lecithin. This effect is particularly evident when comparing the intensity of the diffraction peaks of the particles after 22 days of reaction (see Fig. S2 in the Supplementary Material), *i.e.* the particles prepared in water are more crystalline than the ones obtained in the SIF. Among the components present in the SIF, the stabilizing action is likely due to taurocholate, which is able to inhibit the precipitation of crystalline CaP [27].

The morphology of the amorphous and crystalline samples was studied with scanning electron microscopy (SEM), and the micrographs are reported in Figure 2. When comparing AMCPs collected after 15 min prepared in SIF (Fig. 2a) and water (Fig. 2b), it is clear that the presence of the organic molecules in the SIF affects the morphology of the particles: AMCPs synthesized in this medium appear much smaller and interconnected than the ones obtained from the analogous procedure in water. On the other hand, bobierrite crystals formed upon conversion of AMCPs show the same morphology in both syntheses, namely parallelepiped-like objects surrounded by amorphous particles (see Fig. 2c and d).

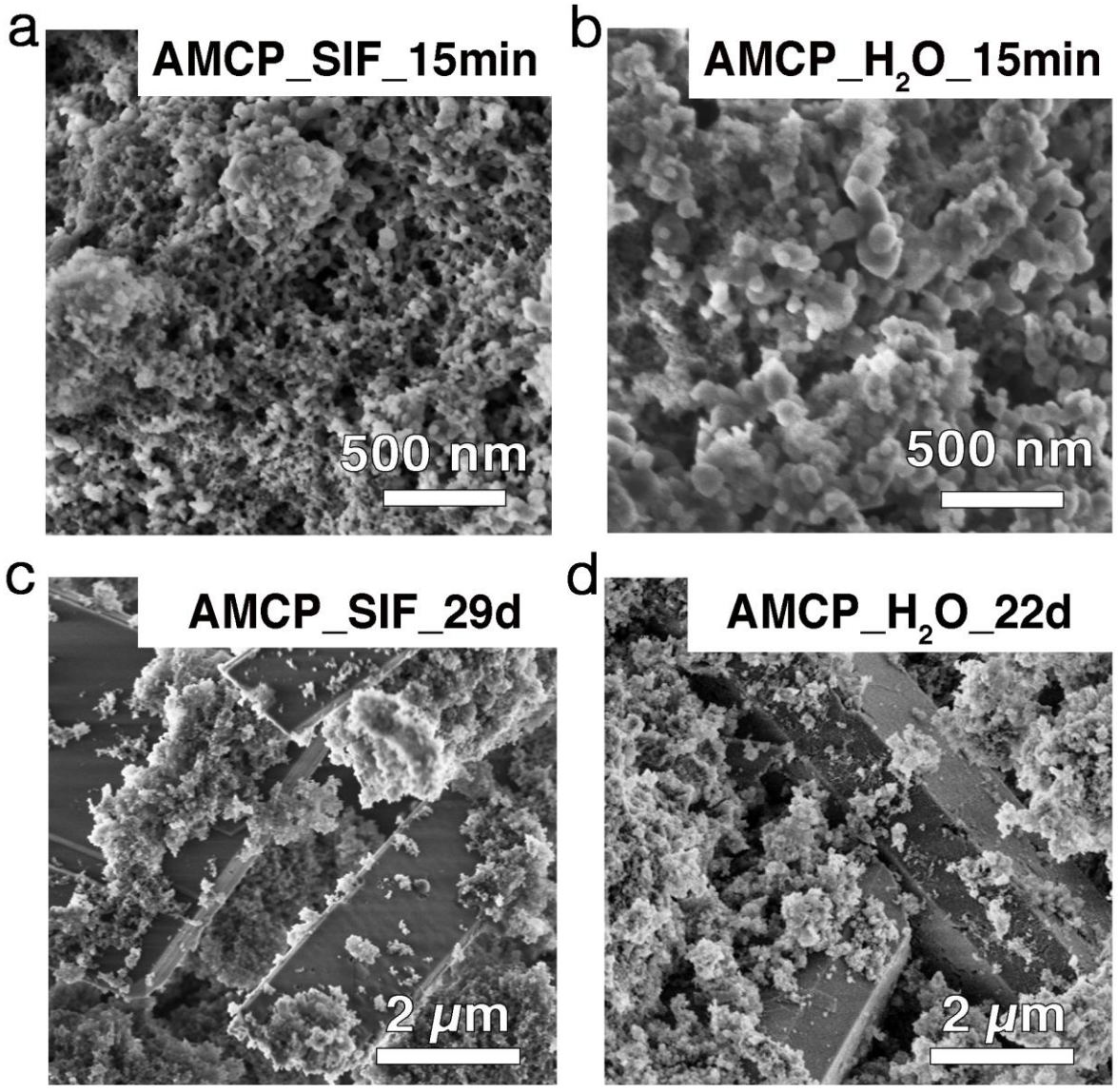

Fig. 2: FE-SEM micrographs of (a) AMCP_SIF_15min; (b) AMCP_H_2O_15min; (c) AMCP_SIF_29d; (d) AMCP_H_2O_22d.

3.3 Incorporation of organic molecules

A peculiar feature of the endogenous AMCPs is their ability to trap antigens and peptidoglycans in the lumen, acting like a shuttle for delivering the organic cargo to the immune cells in the intestinal wall lining [5,45]. The ability of AMCP-like nanoparticles to trap macromolecules during formation was investigated *in vitro* by Pele *et al.*, who found macromolecule-incorporation properties similar to their *in vivo* counterpart [6]. As we observed that the organic molecules present in the SIF affect the morphology of the synthesized particles, we inspected their incorporation/adsorption on AMCPs as a function of time.

By comparing the series of FT-IR spectra of AMCP_SIF (see Fig. 1a) with that of AMCP_H_2O (see Fig. 1b), we found that AMCP_SIF shows an additional peak at 1576 cm^{-1} and, in samples from 3

ACCEPTED MANUSCRIPT

to 10 synthesis days, also present absorptions at 1733 cm^{-1}, 2855 cm^{-1} and 2927 cm^{-1}. These signals can be ascribed to the stretching vibrations of C-C and C-H bonds in lecithin and taurocholate (see Fig. S3 in the Supplementary Material), suggesting the incorporation of these organic molecules in AMCPs. The reason for the different number of peaks in the infrared spectrum as a function of time is probably due to a different amount of organic material, which was estimated by means of thermogravimetry, comparing the weight losses % at 1000 °C. The thermograms are given in Fig. S4a (see the Supplementary Material), and the weight losses as a function of time are shown in Figure 3a. AMCP_SIF samples show a time-dependent weight loss, which is in all cases higher than that of AMCP_H_2O (the weight loss of the particles prepared in water is 19±1% and does not significantly change over time). The higher weight loss observed for AMCPs prepared in SIF is consistent with the thermal degradation of some organic material incorporated into particles: in fact, the TGA profiles of the analyzed samples differ in the extent of the weight losses in the range 200-450 °C, due to the degradation of organic molecules (see the derivative thermogravimetric curves in Fig. S4b).

ACCEPTED MANUSCRIPT

ACCEPTED MANUSCRIPT

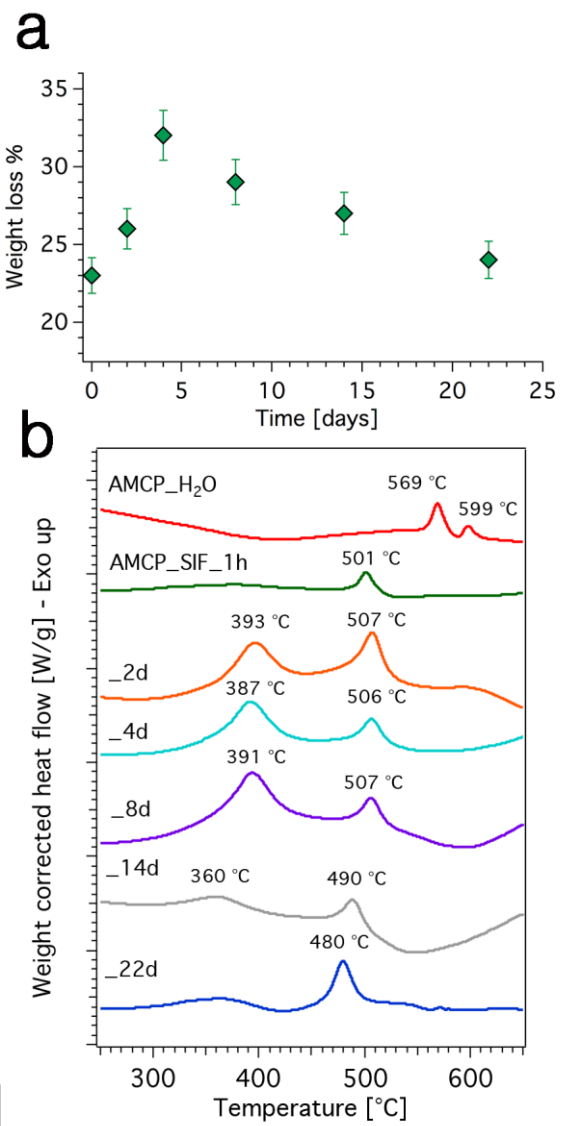

Fig. 3: (a) Weight losses % at 1000 °C of AMCP_SIF as a function of reaction time. The error bars associated to the experimental points, which are the 5% of the value, take into account the discrepancies arising from different measurements on samples obtained from two analogous syntheses. (b) Heat flow profiles of AMCP_SIF, compared with AMCP_H_2O (red curve). The curves are offset for display purposes. The baselines were subtracted using a 3rd order polynomial function.

The amount of organic material in AMCP_SIF samples increases during the early stages of the synthesis, reaches a maximum after ~4 days and then decreases. The samples showing the highest weight losses are the ones displaying, in the FT-IR spectra, the peaks at 1733 cm^{-1}, 2855 cm^{-1} and 2927 cm^{-1}, confirming that these additional infrared features are due to the higher relative amount of organic material in the samples. Some important information can also be obtained from the heat flow profile acquired simultaneously to the thermogravimetry experiments (see Fig. 3b): while heating, two exothermic events appear in the heat flow profile of AMCP_H_2O_15min, which correspond to crystallization processes (conversion to a crystalline sodium calcium magnesium

ACCEPTED MANUSCRIPT

phosphate, see [14]). The amorphous particles prepared in SIF also crystallize when heated, but the exothermic peaks are shifted toward lower temperatures, despite converting to the same phase (see Fig. S5 in the Supplementary Material). As exothermic transitions occur from a less ordered to a more ordered state, the shift to lower temperatures of the peaks indicates that less energy is required for the crystallization to occur for AMCP-SIF samples, suggesting that the amorphous phase is even more disordered than when prepared in water, *i.e.* it is easier for the structural units composing AMCP to re-arrange into a crystalline form.

3.4 AMCP nanostructure

The structure at the nanoscale of AMCPs prepared in SIF was compared to their counterpart obtained in water to investigate if lecithin and taurocholate affect the nanostructure of the amorphous particles. As the endogenous self-assembly of AMCPs constantly occurs in mammalian gut, we inspected the structure of AMCPs obtained after few minutes from the beginning of the reaction, as we expect the *in vivo* formation process to be relatively fast.

TEM micrographs of AMCP_SIF_15min and AMCP_H_2O_15min are compared in Figure 4. The images at lower magnification (Fig. 4a and b) confirm the observations conducted over SEM results, *i.e.* the amorphous particles obtained in SIF (Fig. 4a) are smaller than the ones synthesized in water (Fig. 4b); moreover, in both cases, the nanometric objects are clustered and endowed with nanometric porosities, similarly to the endogenous ones [5]. We verified that particles' agglomeration does not occur on TEM grid as a consequence of sample preparation by analyzing aliquots directly withdrawn from the reacting solution by means of granulometry; the obtained size distributions confirmed that particles' agglomeration occurs in solution (see Fig. S6 in the Supplementary Material).

ACCEPTED MANUSCRIPT

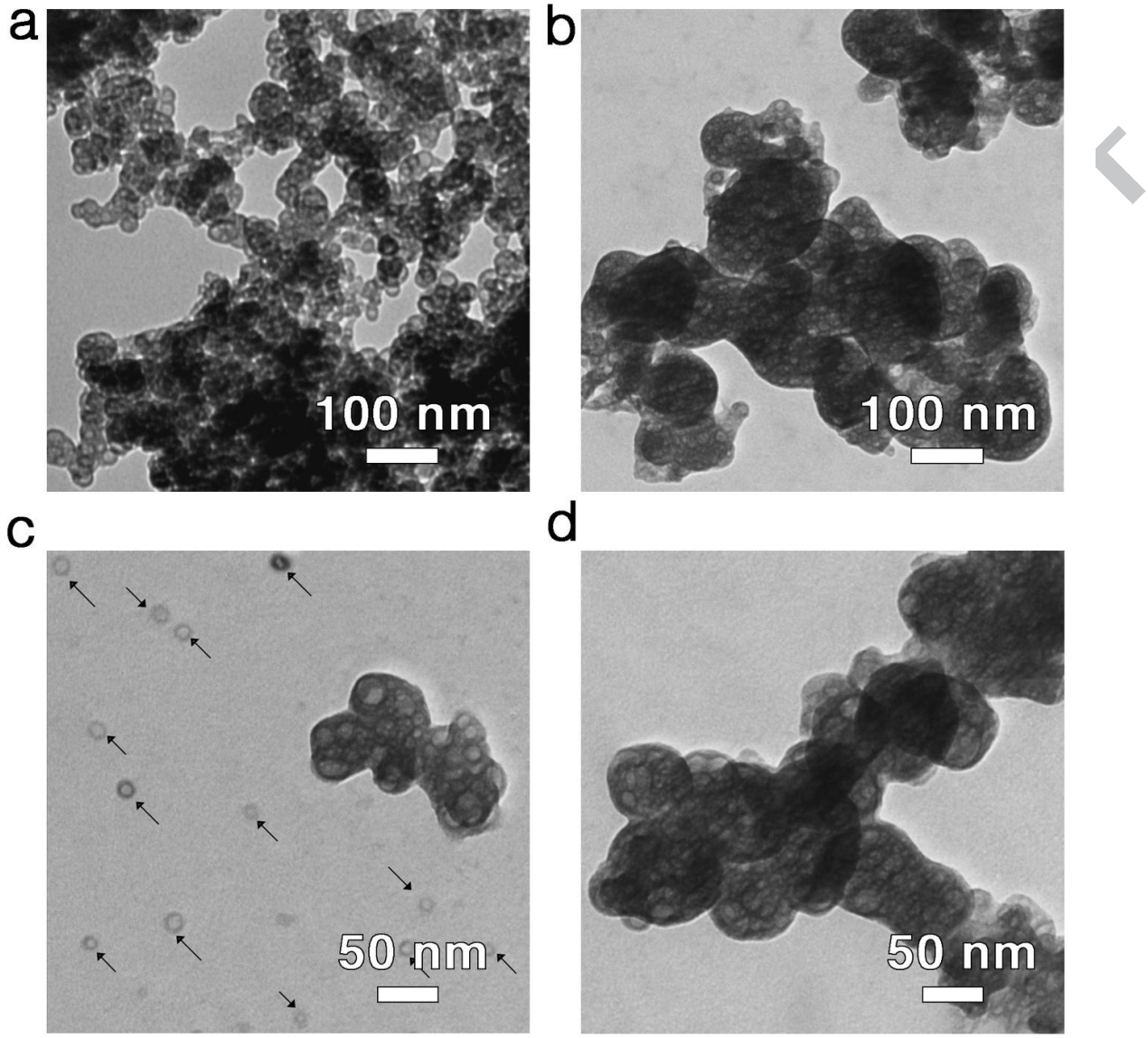

Fig. 4: TEM micrographs of (a + c) AMCP_SIF_15min and (b + d) AMCP_H_2O_15min at low (a+b) and high (c+d) magnification. The black arrows in c highlight the core-shell-like structures.

The high magnification micrographs (Fig. 4c and d) reveal a very peculiar feature of AMCPs prepared in SIF. Together with clustered structures analogous to the ones obtained from the synthesis in water, we can observe isolated core-shell structures (highlighted by the black arrows in Fig. 4 c). These objects have a core diameter of (10 ± 3) nm and a shell thickness of (3 ± 1) nm (see the size distribution in Fig. S7 in the Supplementary Material). As the shell is more electron-dense than the core, we hypothesize that when AMCP self-assemble in the SIF, a portion of the inorganic material forms a shell on the micelles that are present in the fluid (see paragraph 3.1) resulting in core-shell structures. This hypothesis can be supported by the fact that the hydrodynamic diameter obtained by DLS and the core of the objects observed by means of TEM are compatible. In addition, the possibility that the cited objects consist of simple micelles can be excluded,

ACCEPTED MANUSCRIPT

considering that freeze-drying generally leads to the aggregation and/or disruption of self-assembled structures [46,47]; moreover, taurocholate-lecithin micelles are typically observed under cryo-TEM [19,24,48] showing mostly vesicular structures, while here the appearance of the shell suggests the presence of a homogeneous electron-dense material on the outer layer.

Therefore, our findings suggest that at least a part of the organic material, detected by means of FT-IR spectroscopy and TGA, is incorporated in AMCPs thanks to the self-assembled taurocholate/lecithin structures present in solution.

Hollow nanospheres made of calcium phosphate have already been reported in the literature in the presence of several templating agents, such as block copolymers [49,50], lecithin [30], polystyrene [51] and phenol-formaldehyde resin spheres [52], polyelectrolytes [53], amino acids and dipeptides [54], and surfactants [55].

AMCP structure at the nanoscale was further explored by means of SAXS analysis. The curves of both AMCP_SIF_15min and AMCP_H_2O_15min, reported in Figure 5, display a very low scattering intensity at high q values (q > 0.1 $Å^{-1}$) followed by an upturn in the mid- and low-q regions due to the presence of AMCP aggregates.

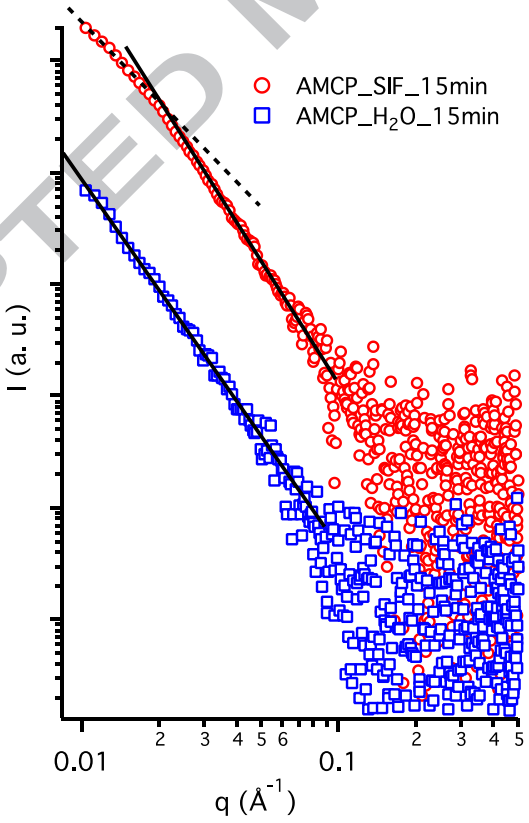

Fig. 5: Log-log representation of SAXS curves of AMCP_SIF_15min (red circles) and AMCP_H_2O_15min (blue squares) samples. Black solid and dashed lines represent curve fittings according to Eq. (1).

ACCEPTED MANUSCRIPT

The presence of core-shell particles as revealed by TEM micrographs on AMCP_SIF_15min sample is not found in the SAXS curve, thus suggesting that the overall scattering intensity is mainly dominated by the aggregates. Filtering AMCP_SIF_15min sample with 0.22 µm filters resulted in a clearer solution, however the SAXS intensity was very low (not shown) and, again, a slight upturn was found at low q values. This indicates that the scattering from the single particle is extremely poor, probably due to low contrast between AMCP and the solvent.

Fitting the AMCP_H_2O_15min linear pattern in the $0.01 > q > 0.1$ $Å^{-1}$ range with Eq. (1) (black solid line in Fig. 5) results in $p = 3.37 \pm 0.01$. According to Eq. (2), this corresponds to a surface-fractal dimension $D_s = 2.63$. For AMCP_SIF_15min, a similar pattern is found in the mid-q region with $p = 3.45 \pm 0.01$ and $D_s = 2.55$, which indicates that, in this dimensional range, the surface of AMCP particles in SIF is slightly rougher than that in water. More interestingly, a second power law dominates the scattering in the low-q region with $p = D_m = 2.37 \pm 0.01$ (black dashed line). The cause of this surface (primary domain) to mass (secondary domain) fractal crossover can be found in the micelles present in SIF structuring the AMCP aggregates into less compact domains. This behavior has been previously reported for particles assembling in solutions and gels when the environment surrounding the particles is changed [56–58], which in our case can be referred to the use of water or SIF as the reaction medium.

4. Conclusions

This work deals with the physico-chemical investigation of the formation and stability of amorphous magnesium-calcium phosphates in a simulated intestinal fluid. The relevance of AMCPs has recently emerged because of the discovery of their endogenous formation in human small intestine. This process, which has a role in the immune-surveillance mechanisms of our organism, is far from being completely understood [5]. As the formation of amorphous calcium phosphates in complex media mimicking intestinal fluids has never been investigated so far, in this study we synthesized AMCPs in a commercial SIF, which specifically reproduces the ileum region of the gut and contains sodium taurocholate and lecithin. The effect of the two separate components on the precipitation of CaPs was barely addressed in the literature [27,28,30,31]; here, we focused our attention on a system containing both molecules in biorelevant conditions, as the simultaneous presence of the two components well mimics the *in vivo* conditions of the ileum. By comparing the features of the obtained particles with the ones of AMCPs produced in water with an analogous method, we found out that the presence of lecithin and taurocholate prolongs the lifetime of the amorphous phase, delaying the conversion of AMCP to bobierrite. This stabilizing action is likely

ACCEPTED MANUSCRIPT

due to the effect of taurocholate, which is known to inhibit the precipitation of crystalline calcium phosphates [27]. The morphology of AMCPs in the two synthetic media is also different, as the particles forming in the SIF are smaller and less aggregated than in water. We also observed that AMCPs are able to incorporate the organic molecules present in the fluid in a time-dependent manner, as shown by means of both FT-IR spectroscopy and thermal analysis. This feature, which is a characteristic of endogenous AMCPs [5], is retained *in vitro* in agreement with previous literature reports [6]. The nanoscale structure of the amorphous particles was further inspected, and TEM analysis revealed a very peculiar structure in AMCPs_SIF: together with clustered particles, it was possible to observe some core-shell structures, with a 10 nm-core and an electron-dense 3 nm-shell. The formation of these objects is likely driven by the presence of self-assembled structures in the SIF with a hydrodynamic radius of 17 nm that we detected by means of DLS. These self-assembled objects possibly are mixed micelles formed by lecithin and sodium taurocholate, which have been described in similar media [19–21,24,25]. Finally, SAXS analysis revealed a different fractal structure for AMCPs synthesized in water or in SIF. In particular, for the latter, a surface-to-mass fractal crossover is found at low scattering vectors, thus revealing distinct aggregation patterns for the two AMCPs in solution. This behavior could influence the crystallization process and consequently provide an explanation to the differences in the temporal stability of the amorphous phases in the two mediums.

As a next step, we aim at addressing the formation of AMCPs in progressively more complex media, exploiting interdisciplinary collaborations with biologists and medics: in fact, a fundamental part of the gut functioning is due to the mutualistic relationship with a huge number of species of microorganisms (both bacteria and fungi). The importance of this flora on the intestinal health is proved and is still an active field of research; the effect of the intestinal microbiota and micobiota on the process of AMCP formation, which is involved in the immunosurveillance mechanisms, is likely to be of great relevance.

Acknowledgements

Fondazione CR Firenze (project 2017.0720) and CSGI consortium are acknowledged for financial support.

ACCEPTED MANUSCRIPT

References

[1] F. Ridi, I. Meazzini, B. Castroflorio, M. Bonini, D. Berti, P. Baglioni, Functional calcium phosphate composites in nanomedicine, Adv. Colloid Interface Sci. 244 (2017) 281–295. doi:10.1016/j.cis.2016.03.006.

[2] G. Tomoaia, R.-D. Pasca, On the Collagen Mineralization. A Review, Clujul Med. 88 (2015) 15–22. doi:10.15386/cjmed-359.

[3] P.-A. Fang, J.F. Conway, H.C. Margolis, J.P. Simmer, E. Beniash, Hierarchical self-assembly of amelogenin and the regulation of biomineralization at the nanoscale, Proc. Natl. Acad. Sci. 108 (2011) 14097–14102. doi:10.1073/pnas.1106228108.

[4] C.N. Rochette, S. Rosenfeldt, A. Heiss, T. Narayanan, M. Ballauff, W. Jahnen-Dechent, A Shielding Topology Stabilizes the Early Stage Protein–Mineral Complexes of Fetuin-A and Calcium Phosphate: A Time-Resolved Small-Angle X-ray Study, ChemBioChem. 10 (2009) 735–740. doi:10.1002/cbic.200800719.

[5] J.J. Powell, E. Thomas-McKay, V. Thoree, J. Robertson, R.E. Hewitt, J.N. Skepper, A. Brown, J.C. Hernandez-Garrido, P.A. Midgley, I. Gomez-Morilla, G.W. Grime, K.J. Kirkby, N.A. Mabbott, D.S. Donaldson, I.R. Williams, D. Rios, S.E. Girardin, C.T. Haas, S.F.A. Bruggraber, J.D. Laman, Y. Tanriver, G. Lombardi, R. Lechler, R.P.H. Thompson, L.C. Pele, An endogenous nanomineral chaperones luminal antigen and peptidoglycan to intestinal immune cells, Nat. Nanotechnol. 10 (2015) 361–369. doi:10.1038/nnano.2015.19.

[6] L.C. Pele, C.T. Haas, R.E. Hewitt, J. Robertson, J. Skepper, A. Brown, J.C. Hernandez-Garrido, P.A. Midgley, N. Faria, H. Chappell, J.J. Powell, Synthetic mimetics of the endogenous gastrointestinal nanomineral: Silent constructs that trap macromolecules for intracellular delivery, Nanomedicine Nanotechnol. Biol. Med. 13 (2017) 619–630. doi:10.1016/j.nano.2016.07.008.

[7] M. Nabiyouni, T. Brückner, H. Zhou, U. Gbureck, S.B. Bhaduri, Magnesium-based bioceramics in orthopedic applications, Acta Biomater. 66 (2018) 23–43. doi:10.1016/j.actbio.2017.11.033.

[8] U. Klammert, T. Reuther, M. Blank, I. Reske, J.E. Barralet, L.M. Grover, A.C. Kübler, U. Gbureck, Phase composition, mechanical performance and in vitro biocompatibility of hydraulic setting calcium magnesium phosphate cement, Acta Biomater. 6 (2010) 1529–1535. doi:10.1016/j.actbio.2009.10.021.

[9] F. Tamimi, D.L. Nihouannen, D.C. Bassett, S. Ibasco, U. Gbureck, J. Knowles, A. Wright, A. Flynn, S.V. Komarova, J.E. Barralet, Biocompatibility of magnesium phosphate minerals and

ACCEPTED MANUSCRIPT

their stability under physiological conditions, Acta Biomater. 7 (2011) 2678–2685. doi:10.1016/j.actbio.2011.02.007.

[10] E. Babaie, B. Lin, V.K. Goel, S.B. Bhaduri, Evaluation of amorphous magnesium phosphate (AMP) based non-exothermic orthopedic cements, Biomed. Mater. 11 (2016) 055010. doi:10.1088/1748-6041/11/5/055010.

[11] C. Combes, C. Rey, Amorphous calcium phosphates: Synthesis, properties and uses in biomaterials, Acta Biomater. 6 (2010) 3362–3378. doi:10.1016/j.actbio.2010.02.017.

[12] S.V. Dorozhkin, Amorphous calcium (ortho)phosphates, Acta Biomater. 6 (2010) 4457–4475. doi:10.1016/j.actbio.2010.06.031.

[13] A.L. Boskey, A.S. Posner, Magnesium stabilization of amorphous calcium phosphate: A kinetic study, Mater. Res. Bull. 9 (1974) 907–916. doi:10.1016/0025-5408(74)90169-X.

[14] R. Gelli, M. Scudero, L. Gigli, M. Severi, M. Bonini, F. Ridi, P. Baglioni, Effect of pH and Mg2+ on Amorphous Magnesium-Calcium Phosphate (AMCP) stability, J. Colloid Interface Sci. 531 (2018) 681–692. doi:10.1016/j.jcis.2018.07.102.

[15] D. Riethorst, R. Mols, G. Duchateau, J. Tack, J. Brouwers, P. Augustijns, Characterization of Human Duodenal Fluids in Fasted and Fed State Conditions, J. Pharm. Sci. 105 (2016) 673–681. doi:10.1002/jps.24603.

[16] K. Kleberg, J. Jacobsen, A. Müllertz, Characterising the behaviour of poorly water soluble drugs in the intestine: application of biorelevant media for solubility, dissolution and transport studies, J. Pharm. Pharmacol. 62 (2010) 1656–1668. doi:10.1111/j.2042-7158.2010.01023.x.

[17] C.A.S. Bergström, R. Holm, S.A. Jørgensen, S.B.E. Andersson, P. Artursson, S. Beato, A. Borde, K. Box, M. Brewster, J. Dressman, K.-I. Feng, G. Halbert, E. Kostewicz, M. McAllister, U. Muenster, J. Thinnes, R. Taylor, A. Mullertz, Early pharmaceutical profiling to predict oral drug absorption: Current status and unmet needs, Eur. J. Pharm. Sci. 57 (2014) 173–199. doi:10.1016/j.ejps.2013.10.015.

[18] C. Markopoulos, C.J. Andreas, M. Vertzoni, J. Dressman, C. Reppas, In-vitro simulation of luminal conditions for evaluation of performance of oral drug products: Choosing the appropriate test media, Eur. J. Pharm. Biopharm. 93 (2015) 173–182. doi:10.1016/j.ejpb.2015.03.009.

[19] B. Kloefer, P. van Hoogevest, R. Moloney, M. Kuentz, M.L.S. Leigh, J. Dressman, Study of a Standardized Taurocholate– Lecithin Powder for Preparing the Biorelevant Media FeSSIF and FaSSIF, Dissolution Technol. 17 (2010) 6–13. doi:10.14227/DT170310P6.

ACCEPTED MANUSCRIPT

[20] M.C. di Gregorio, L. Travaglini, A. Del Giudice, J. Cautela, N.V. Pavel, L. Galantini, Bile Salts: Natural Surfactants and Precursors of a Broad Family of Complex Amphiphiles, Langmuir. (2018). doi:10.1021/acs.langmuir.8b02657.

[21] R. Holm, A. Müllertz, H. Mu, Bile salts and their importance for drug absorption, Int. J. Pharm. 453 (2013) 44–55. doi:10.1016/j.ijpharm.2013.04.003.

[22] C.-Y. Cheng, H. Oh, T.-Y. Wang, S.R. Raghavan, S.-H. Tung, Mixtures of Lecithin and Bile Salt Can Form Highly Viscous Wormlike Micellar Solutions in Water, Langmuir. 30 (2014) 10221–10230. doi:10.1021/la502380q.

[23] J. Cautela, M. Giustini, N.V. Pavel, G. Palazzo, L. Galantini, Wormlike reverse micelles in lecithin/bile salt/water mixtures in oil, Colloids Surf. Physicochem. Eng. Asp. 532 (2017) 411–419. doi:10.1016/j.colsurfa.2017.04.052.

[24] K. Kleberg, F. Jacobsen, D.G. Fatouros, A. Müllertz, Biorelevant Media Simulating Fed State Intestinal Fluids: Colloid Phase Characterization and Impact on Solubilization Capacity, J. Pharm. Sci. 99 (2010) 3522–3532. doi:10.1002/jps.22122.

[25] G.A. Kossena, B.J. Boyd, C.J.H. Porter, W.N. Charman, Separation and Characterization of the Colloidal Phases Produced on Digestion of Common Formulation Lipids and Assessment of Their Impact on the Apparent Solubility of Selected Poorly Water-Soluble Drugs, J. Pharm. Sci. 92 (2003) 634–648. doi:10.1002/jps.10329.

[26] D.J. Sutor, J.M. Percival, Presence or absence of inhibitors of crystal growth in bile. 1. Effect of bile on the formation of calcium phosphate, a constituent of gallstones., Gut. 17 (1976) 506–510. doi:10.1136/gut.17.7.506.

[27] E.W. Moore, L. Celic, J.D. Ostrow, Interactions between ionized calcium and sodium taurocholate: bile salts are important buffers for prevention of calcium-containing gallstones, Gastroenterology. 83 (1982) 1079–1089. doi:10.1016/S0016-5085(82)80077-2.

[28] R.S. Crowther, M. Okido, Inhibition of calcium phosphate precipitation by bile salts: a test of the Ca(2+)-buffering hypothesis, J. Lipid Res. 35 (1994) 279–290.

[29] M. Okido, R.D. Soloway, R.S. Crowther, Influence of phospholipid on bile salt binding to calcium hydroxyapatite and on the poisoning of nascent hydroxyapatite crystals, Liver. 16 (1996) 321–325. doi:10.1111/j.1600-0676.1996.tb00753.x.

[30] G.-J. Ding, Y.-J. Zhu, C. Qi, B.-Q. Lu, F. Chen, J. Wu, Porous hollow microspheres of amorphous calcium phosphate: soybean lecithin templated microwave-assisted hydrothermal synthesis and application in drug delivery, J. Mater. Chem. B. 3 (2015) 1823–1830. doi:10.1039/C4TB01862A.

ACCEPTED MANUSCRIPT

[31] W. Michał, D. Ewa, C. Tomasz, Lecithin-based wet chemical precipitation of hydroxyapatite nanoparticles, Colloid Polym. Sci. 293 (2015) 1561–1568. doi:10.1007/s00396-015-3557-0.

[32] C. Holt, M. Van Kemenade, J.E. Harries, L.S. Nelson, R.T. Bailey, D.W.L. Hukins, S.S. Hasnain, P.L. De Bruyn, Preparation of amorphous calcium-magnesium phosphates at pH 7 and characterization by x-ray absorption and fourier transform infrared spectroscopy, J. Cryst. Growth. 92 (1988) 239–252. doi:10.1016/0022-0248(88)90455-1.

[33] H.M. Fadda, A.W. Basit, Dissolution of pH responsive formulations in media resembling intestinal fluids: bicarbonate versus phosphate buffers, J. Drug Deliv. Sci. Technol. 15 (2005) 273–279. doi:10.1016/S1773-2247(05)50049-2.

[34] J. Aron-Wisnewsky, J. Doré, K. Clement, The importance of the gut microbiota after bariatric surgery, Nat. Rev. Gastroenterol. Hepatol. 9 (2012) 590. doi:10.1038/nrgastro.2012.161.

[35] J.A. Lake, An iterative method of slit-correcting small angle X-ray data, Acta Crystallogr. 23 (1967) 191–194. doi:10.1107/S0365110X67002440.

[36] B. Hammouda, Probing Nanoscale Structures - The SANS Toolbox, Https://Www.Ncnr.Nist.Gov/Staff/Hammouda/The_SANS_toolbox.Pdf. (2012).

[37] D.W. Schaefer, Fractal Models and the Structure of Materials, MRS Bull. 13 (1988) 22–27. doi:10.1557/S088376940006632X.

[38] S. V. Dorozhkin, Amorphous Calcium Orthophosphates: Nature, Chemistry and Biomedical Applications, Int. J. Mater. Chem. 2 (2012) 19–46. doi:10.5923/j.ijmc.20120201.04.

[39] C. Drouet, Apatite Formation: Why It May Not Work as Planned, and How to Conclusively Identify Apatite Compounds, BioMed Res. Int. 2013 (2013) 490946. doi:10.1155/2013/490946.

[40] C. Holt, M.J.J.M. Van Kemenade, L.S. Nelson, D.W.L. Hukins, R.T. Bailey, J.E. Harries, S.S. Hasnain, P.L. De Bruyn, Amorphous calcium phosphates prepared at pH 6.5 and 6.0, Mater. Res. Bull. 24 (1989) 55–62. doi:10.1016/0025-5408(89)90008-1.

[41] A.C. Tas, X-ray-amorphous calcium phosphate (ACP) synthesis in a simple biomineralization medium, J. Mater. Chem. B. 1 (2013) 4511. doi:10.1039/c3tb20854k.

[42] M.H. Salimi, J.C. Heughebaert, G.H. Nancollas, Crystal growth of calcium phosphates in the presence of magnesium ions, Langmuir. 1 (1985) 119–122. doi:10.1021/la00061a019.

[43] E. Babaie, B. Lin, S.B. Bhaduri, A new method to produce macroporous Mg-phosphate bone growth substitutes, Mater. Sci. Eng. C. 75 (2017) 602–609. doi:10.1016/j.msec.2017.02.111.

ACCEPTED MANUSCRIPT

[44] M.A. Rivadeneyra, A. Ramos-Cormenzana, A. Garcia-Cervigon, Formation of bobierrite (magnesium phosphate) crystal aggregates by Acinetobacter sp., Mineral. J. 13 (1987) 443–447. doi:10.2465/minerj.13.443.

[45] J.D. Söderholm, Gut immunology: Nanoparticles ferry gut antigens, Nat. Nanotechnol. 10 (2015) 298–299. doi:10.1038/nnano.2015.58.

[46] J. Logie, S.C. Owen, C.K. McLaughlin, M.S. Shoichet, PEG-Graft Density Controls Polymeric Nanoparticle Micelle Stability, Chem. Mater. 26 (2014) 2847–2855. doi:10.1021/cm500448x.

[47] C. Di Tommaso, C. Como, R. Gurny, M. Möller, Investigations on the lyophilisation of MPEG–hexPLA micelle based pharmaceutical formulations, Eur. J. Pharm. Sci. 40 (2010) 38–47. doi:10.1016/j.ejps.2010.02.006.

[48] D.G. Fatouros, I. Walrand, B. Bergenstahl, A. Müllertz, Colloidal Structures in Media Simulating Intestinal Fed State Conditions with and Without Lipolysis Products, Pharm. Res. 26 (2009) 361–374. doi:10.1007/s11095-008-9750-9.

[49] B.P. Bastakoti, M. Inuoe, S. Yusa, S.-H. Liao, K.C.-W. Wu, K. Nakashima, Y. Yamauchi, A block copolymer micelle template for synthesis of hollow calcium phosphate nanospheres with excellent biocompatibility, Chem. Commun. 48 (2012) 6532–6534. doi:10.1039/C2CC32279J.

[50] W. Tjandra, P. Ravi, J. Yao, K.C. Tam, Synthesis of hollow spherical calcium phosphate nanoparticles using polymeric nanotemplates, Nanotechnol. Print. 17 (2006) 5988–5994. doi:10.1088/0957-4484/17/24/014.

[51] C. Wu, J. Xu, Y. Hao, Y. Zhao, Y. Qiu, J. Jiang, T. Yu, P. Ji, Y. Liu, Application of a lipid-coated hollow calcium phosphate nanoparticle in synergistic co-delivery of doxorubicin and paclitaxel for the treatment of human lung cancer A549 cells, Int. J. Nanomedicine. 12 (2017) 7979–7992. doi:10.2147/IJN.S140957.

[52] S. Huang, C. Li, Q. Xiao, Tunable pore sizes of monodispersed amorphous calcium phosphate hollow nanospheres, Mater. Lett. 197 (2017) 1–4. doi:10.1016/j.matlet.2017.03.069.

[53] A. Bigi, E. Boanini, D. Walsh, S. Mann, Morphosynthesis of Octacalcium Phosphate Hollow Microspheres by Polyelectrolyte-Mediated Crystallization, Angew. Chem. 114 (2002) 2267–2270. doi:10.1002/1521-3757(20020617)114:12<2267::AID-ANGE2267>3.0.CO;2-N.

[54] D. Hagmeyer, K. Ganesan, J. Ruesing, D. Schunk, C. Mayer, A. Dey, N.A.J. M. Sommerdijk, M. Epple, Self-assembly of calcium phosphate nanoparticles into hollow spheres induced by dissolved amino acids, J. Mater. Chem. 21 (2011) 9219–9223. doi:10.1039/C1JM11316J.

ACCEPTED MANUSCRIPT

[55] Y. Cai, H. Pan, X. Xu, Q. Hu, L. Li, R. Tang, Ultrasonic Controlled Morphology Transformation of Hollow Calcium Phosphate Nanospheres: A Smart and Biocompatible Drug Release System, Chem. Mater. 19 (2007) 3081–3083. doi:10.1021/cm070298t.

[56] A.P. Perissinotto, C.M. Awano, D.A. Donatti, F.S. de Vicente, D.R. Vollet, Mass and Surface Fractal in Supercritical Dried Silica Aerogels Prepared with Additions of Sodium Dodecyl Sulfate, Langmuir. 31 (2015) 562–568. doi:10.1021/la504272g.

[57] P. Wong, Q. Cao, Correlation function and structure factor for a mass fractal bounded by a surface fractal, Phys. Rev. B. 45 (1992) 7627–7632. doi:10.1103/PhysRevB.45.7627.

[58] P. Tempesti, G.S. Nicotera, M. Bonini, E. Fratini, P. Baglioni, Poly(N-isopropylacrylamide)-hydroxyapatite nanocomposites as thermoresponsive filling materials on dentinal surface and tubules, J. Colloid Interface Sci. 509 (2018) 123–131. doi:10.1016/j.jcis.2017.09.001.

ACCEPTED MANUSCRIPT

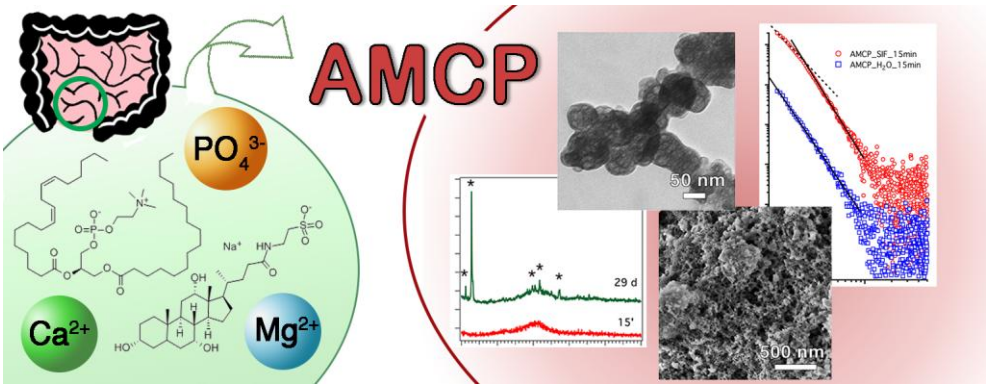

ACCEPTED MANUSCRIPT